Electronic supplementary information:

Effect of halide ratio and Cs^+ addition on the photochemical stability of lead halide perovskites

Sebastian Svanström,[a] T. Jesper Jacobsson,[b] Tamara Sloboda,[c] Erika Giangrisostomi,[d] Ruslan Ovsyannikov,[d] Håkan Rensmo,[a] Ute B. Cappel[c,*]

[a] Division of Molecular and Condensed Matter Physics, Department of Physics and Astronomy, Uppsala University, Box 516, SE-751 20 Uppsala, Sweden

[b] Department of Chemistry –Ångström Laboratory, Uppsala University, Box 538, 75121 Uppsala, Sweden

[c] Division of Applied Physical Chemistry, Department of Chemistry, KTH Royal Institute of Technology, SE-100 44 Stockholm, Sweden

[d] Institute Methods and Instrumentation for Synchrotron Radiation Research, Helmholtz-Zentrum Berlin GmbH, Albert-Einstein-Straße 15, 12489 Berlin, Germany

*cappel@kth.se

Sample preparation

FTO substrates were cleaned in an ultrasound bath in three 30 minutes steps with RBS™ 50 detergent, ethanol, and finally acetone. The substrates were subsequently treated in a UV-ozone cleaner for 10 minutes. An electron transport layer of TiO_2 was deposited on the cleaned FTO substrates using spray pyrolysis. The spray solution consisted of ethanol, acetyl acetone and titanium diisopropoxide (30% in isopropanol) in the proportions of 90:4:6 by volume. Air at a base pressure of 1 bar was used as a carrier gas. The FTO substrates were heated to 450 °C on a hotplate and kept at that temperature for 15 minutes prior to the spraying. After an additional 30 minutes at 450 °C, the sprayed glass substrates were slowly cooled to room temperature. 10 ml of spray solution was used to cover 200 cm^2 of substrates. This procedure gives a compact layer of anatase with a thickness of around 20-30 nm.

On top of the compact TiO_2-layer, a mesoporous layer of TiO_2 nanoparticles was deposited by spin-coating. TiO_2 paste (30 NR-D) was bought from Great Cell Solar and was dissolved in ethanol at a concentration of 150 mg/ml. On each substrate (1.4·2.4 cm), 50 µl of the TiO_2 solution was applied and spin-coated at 4000 rpm with an acceleration of 2000 rpm/s for 10 s. A piece of scotch tape was used on one side of the substrates to prevent the mesoporous TiO_2 to form where the front contacts were to be deposited for complete solar cells. The substrates with mesoporous TiO_2 were sintered at 450 °C in air on a hot plate for 30 minutes and then slowly cooled to ambient temperature.

Prior to perovskite deposition, the substrates with mesoporous TiO_2 underwent a lithium treatment which has been found to be beneficial for the device performance [1]. On the substrates, 100 µl of a 35 mM lithium bistrifluoromethanesulfonimidate (Li-TFSI) in acetonitrile was applied and spun at 3000 rpm for 10 s. The substrates were thermally annealed in air at 450 °C for 30 minutes and then slowly cooled to 150 °C. After annealing, they were transferred directly into a glovebox for perovskite deposition.

The perovskite precursor solutions were spin-coated in a nitrogen-filled glove box. For each sample, 40 µl precursor solution was spread over the substrate and then spin-coated using a two-step program. The first step was a spreading step using a rotation speed of 1000 rpm with an acceleration of 200 rpm/s for 10 s. That step was immediately (without pause) followed by the second step where the films were spun at 6000 rpm for 20 s using an acceleration of 2000 rpm/s. During the second step, when approximately 5 seconds of the program remained, 100 µl of anhydrous chlorobenzene were applied on the spinning film with a hand held automatic pipette. This last step, known as the anti-solvent method, has a large impact on film morphology and results in significantly better device performances [2]–[4]. Directly after spin-coating, the films were placed on a hotplate at 100 °C where they were annealed for 30-70 min.

After annealing, the samples were cooled to ambient temperature. For solar cells, a solution of the solid state hole-conductor ,2'7,7'-tetrakis-(*N,N*-di-*p*-methoxyphenyl-amine)-9,9'-spirobifluorene (spiro) was then spin-coated on top of the films. A 70 mM spiro in chlorobenzene was used to prepare the hole conductor layer. To improve the performance of spiro, three different additives were added [5], [6]: 4-*tert*-butylpyridine, 1.8 M Li-TFSI in acetonitrile, and 0.25 M Co[t-BuPyPz]$_3$[TFSI]$_3$, also known as FK209, in acetonitrile. The Spiro:FK209:Li-TFSI:TBP molar ratio was 1:0.05:0.5:3.3. The spiro solution was prepared and deposited on the same day as the perovskite films were deposited.

The spiro film was prepared by spin-coating at 4000 rpm for 20 s. 50 µl of the solution were deposited on the spinning film using a hand held automatic pipet a few seconds into the spinning program. The samples were stored in a desiccator with silica gel.

Before the back contact was deposited, the perovskite/spiro layer was removed from one end of the samples using a razorblade, acetonitrile, and a cotton bud. An 80 nm thick gold film was deposited by vapour deposition at a pressure of around $2 \cdot 10^{-5}$ Torr as a back contact.

UV-vis and PL

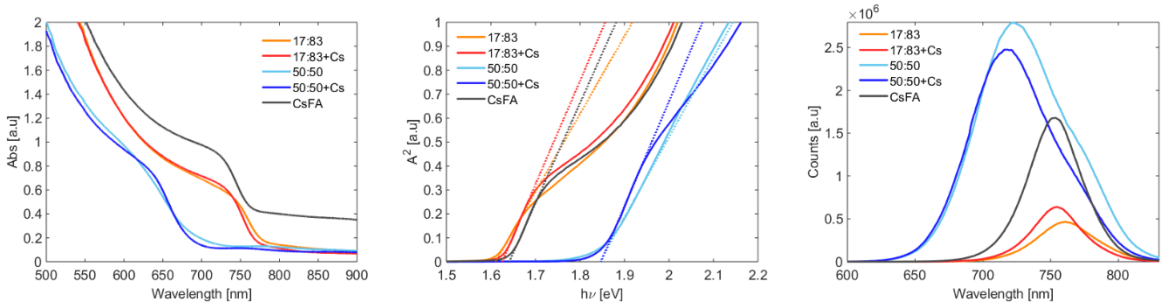

Figure S1: (a) Absorption spectra. Raw data. The higher background of the CsFA samples is due to more reflections/scattering, which is likely correlated to an increased surface roughness. (b) Graphical representation of how the band gaps were extracted. (c) Steady state fluorescence spectra. Not normalised.

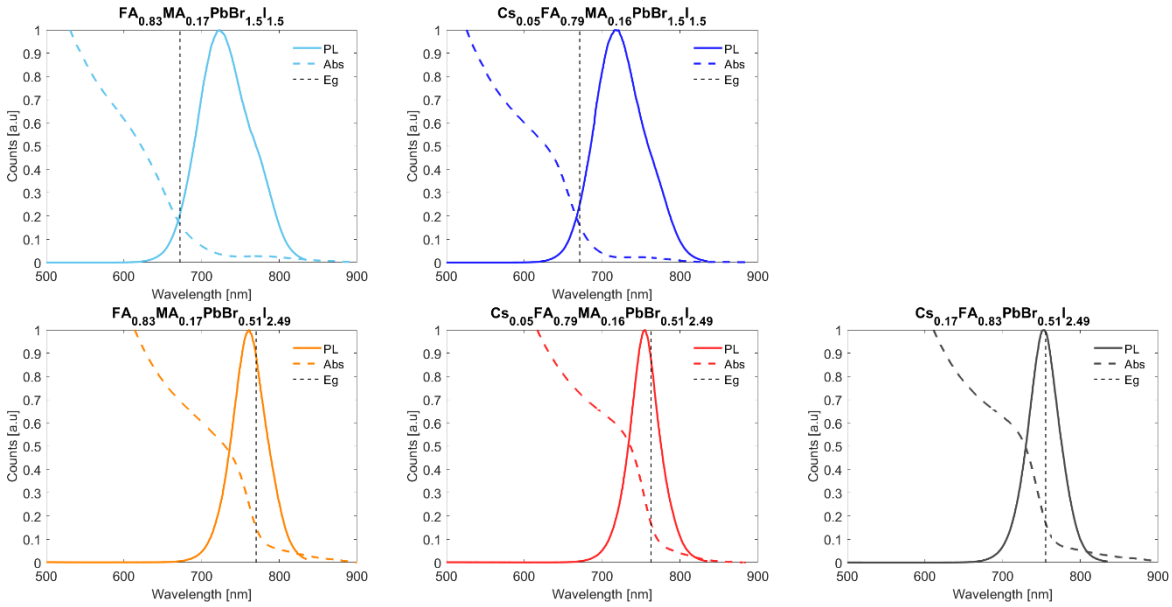

Figure S2: Comparison of absorption data, steady state fluorescence and the extracted band gap for the investigated compositions.

XRD

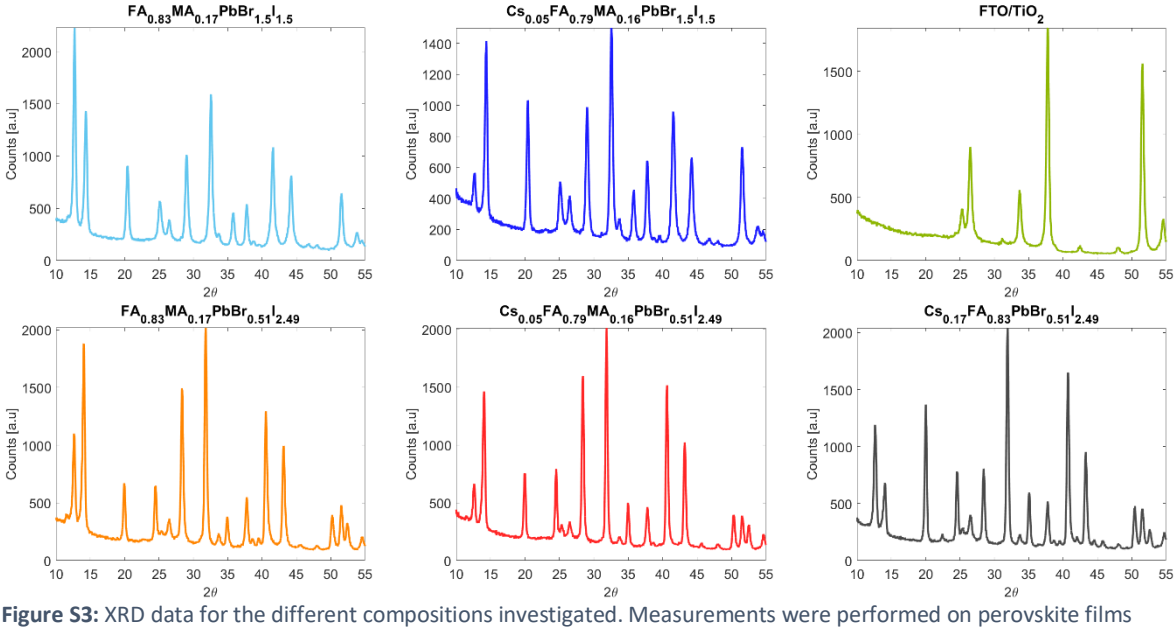

Figure S3: XRD data for the different compositions investigated. Measurements were performed on perovskite films deposited on FTO/TiO_2.

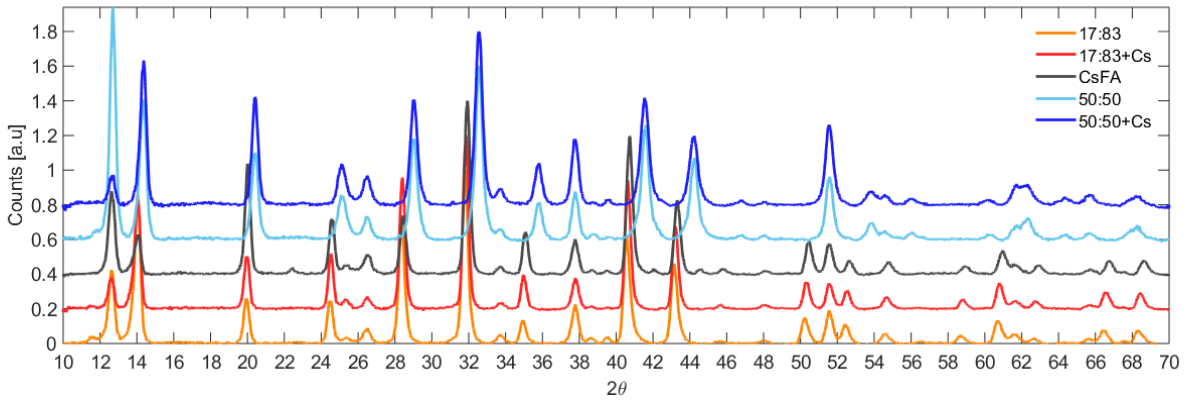

Figure S4: Comparison of the XRD diffractograms in Figure S3.

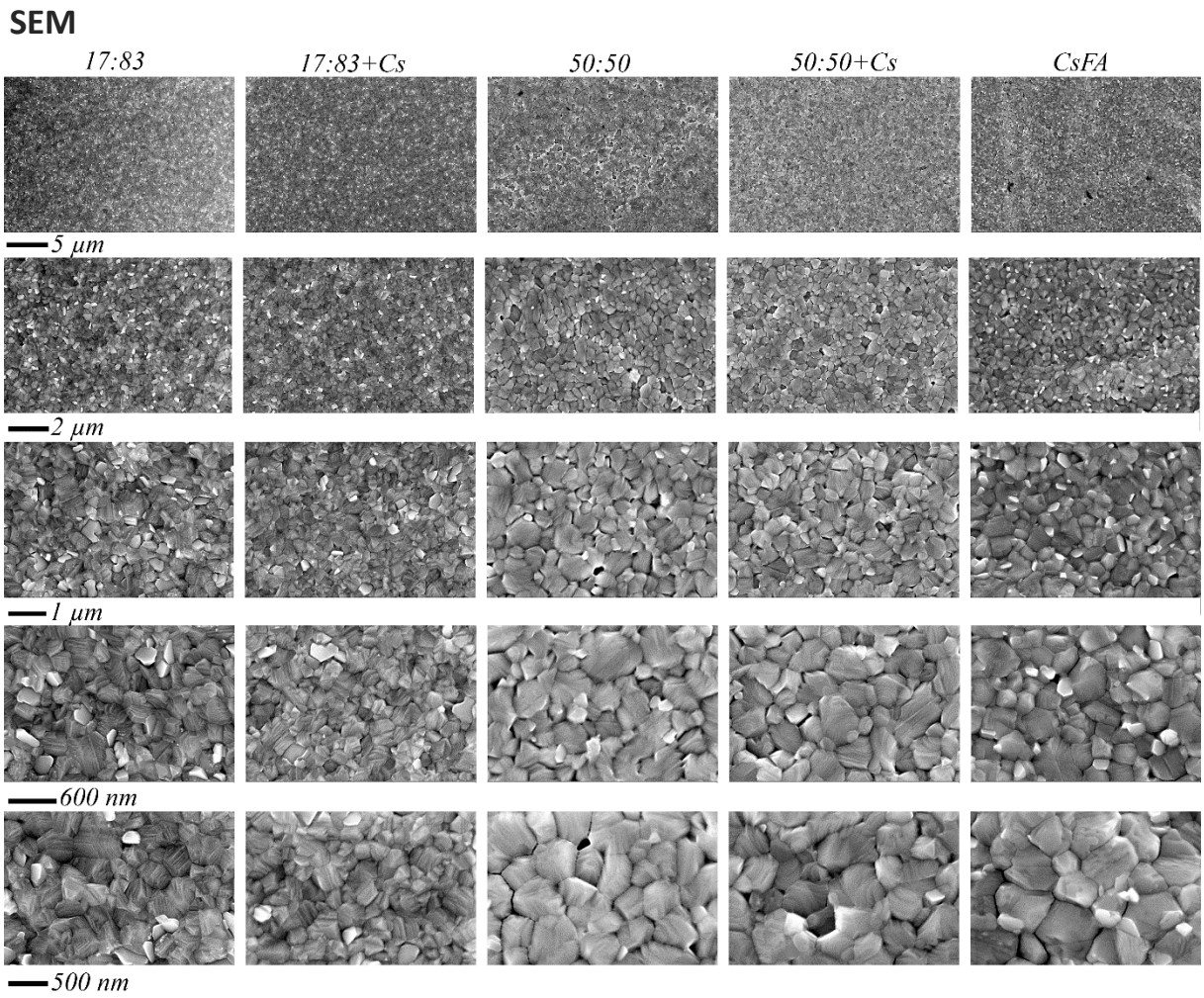

Figure S5: Top view SEM images at different magnifications of the five different compositions explored.

Device characterisation

The IV-characteristics of the solar cells were measured using a home-built system. To simulate solar light, a Newport solar simulator (model 91160) with a xenon arc lamp, fed with 230 W input power and a AM 1.5 filter. The light intensity was calibrated with a silicon photodiode. The IV-curves were measured with a digital source meter (Keithley 2400). No equilibration time or light soaking was applied before the potential scan. The starting point for the measurements was chosen as V_{oc} + 0.05 V. The potential was then scanned to short circuit and back again using a scan speed of 20 mV/s. Thereafter, the dark current was recorded using the same scan speed. The solar cells were masked with a metal mask in order to limit the active cell area to 0.126 cm^2.

Table S1: Summary of device data for the solar cells measured. Data is of the best sub cell (of two) on each substrate. One cell of each composition was made.

Composition	Name	η_b [%]	Voc_b [V]	Jsc_b [mA/cm²]	FF_b [%]	H	η_f [%]	Voc_f [V]	Jsc_f [mA/cm²]	FF_f [%]
$FA_{0.83}MA_{0.17}PbBr_{1.5}I_{1.5}$	50:50	9.9	1.04	15.5	0.62	0.21	6.4	0.98	15.3	0.43
$Cs_{0.05}FA_{0.79}MA_{0.16}PbBr_{1.5}I_{1.5}$	50:50+Cs	11.2	1.02	16.3	0.68	0.26	6.3	0.96	16.4	0.40
$FA_{0.83}MA_{0.17}PbBr_{0.51}I_{2.49}$	17:83	17.0	1.08	21.9	0.71	0.09	14.1	1.04	22.0	0.62
$Cs_{0.05}FA_{0.79}$ $MA_{0.16}PbBr_{0.51}I_{2.49}$	17:83+Cs	17.1	1.04	22.0	0.74	0.12	13.4	1.02	22.2	0.60
$Cs_{0.17}FA_{0.83}PbBr_{0.51}I_{2.49}$	CsFA	15.0	1.02	21.6	0.68	0.11	11.6	1.02	21.6	0.53

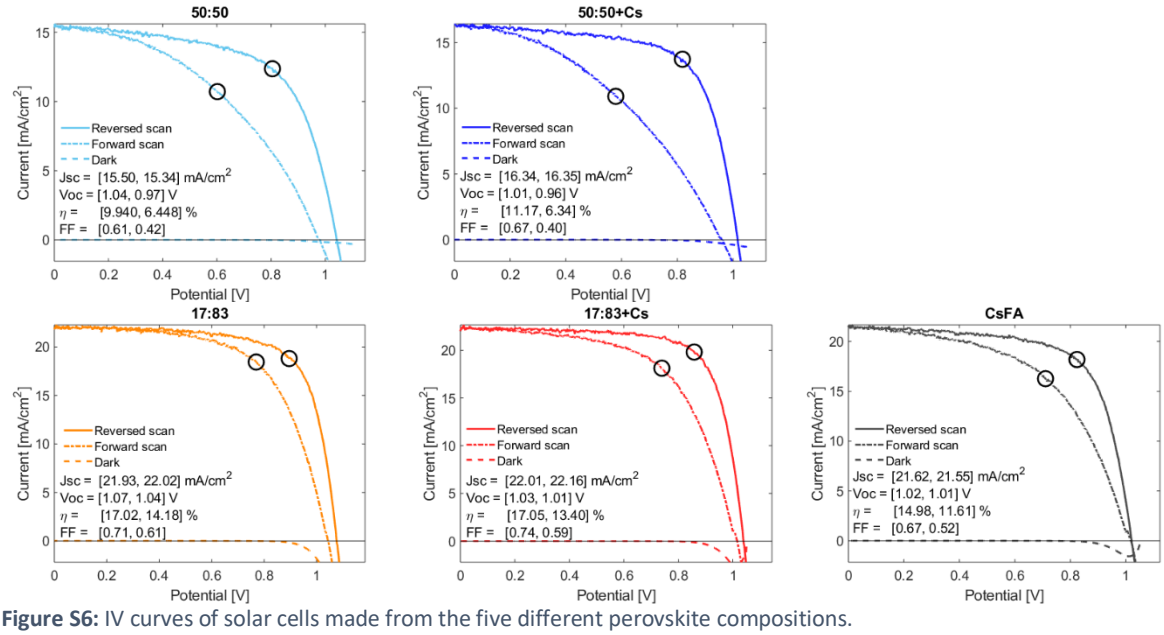

Figure S6: IV curves of solar cells made from the five different perovskite compositions.

Sample characterisation

Table S2: I/Pb(+II) and Br/Pb(+II) ratios of the perovskite samples at 120 eV, 139 eV, 147 eV and 540 eV before and after laser illumination for 30 minutes with 0.2 mW (after illumination is denoted with an L). The ratios are corrected against PbI_2 and $PbBr_2$ reference samples by setting the I/Pb(+II) and Br/Pb(II) ratio of the reference samples to 2.

Reference	**120 eV**		**139 eV**		**147 eV**		**540 eV**	
	I/Pb(II)	Br/Pb(II)	I/Pb(II)	Br/Pb(II)	I/Pb(II)	Br/Pb(II)	I/Pb(II)	Br/Pb(II)
PbI_2	4.90	-	3.67	-	2.66	-	2.51	-
Correction	0.41	-	0.54	-	0.75	-	0.80	-
$PbBr_2$	-	0.41	-	0.46	-	0.49	-	3.09
Correction	-	4.88	-	4.35	-	4.08	-	0.65
Measured	I/Pb(II)	Br/Pb(II)	I/Pb(II)	Br/Pb(II)	I/Pb(II)	Br/Pb(II)	I/Pb(II)	Br/Pb(II)
17:83	7.23	0.09	5.80	0.11	-	-	4.20	0.56
17:83 (L)	9.10	0.17	7.01	0.22	-	-	4.72	1.01
17:83+Cs	7.97	0.08	5.50	0.10	4.39	0.12	4.24	0.60
17:83+Cs (L)	7.97	0.07	5.74	0.10	4.33	0.11	4.23	0.58
50:50	5.32	0.31	4.21	0.40	-	-	2.73	2.52
50:50 (L)	4.30	0.59	3.12	0.71	-	-	2.17	3.37
50:50+Cs	5.78	0.34	4.29	0.38	3.24	0.44	2.73	2.29
50:50+Cs (L)	5.78	0.47	3.59	0.63	2.52	0.72	2.31	3.08
CsFA	7.22	-	5.17	0.04	4.16	0.06	3.89	0.39
CsFA (L)	7.12	-	5.59	0.05	4.00	0.06	3.85	0.37
Corrected	I/Pb(II)	Br/Pb(II)	I/Pb(II)	Br/Pb(II)	I/Pb(II)	Br/Pb(II)	I/Pb(II)	Br/Pb(II)
PbI_2	2.00	-	2.00	-	2.00	-	2.00	-
$PbBr_2$	-	2.00	-	2.00	-	2.00	-	2.00
17:83	2.95	0.42	3.16	0.48	-	-	3.35	0.36
17:83 (L)	3.71	0.81	3.82	0.96	-	-	3.76	0.65
17:83+Cs	3.25	0.40	3.00	0.43	3.30	0.49	3.38	0.39
17:83+Cs (L)	3.25	0.35	3.13	0.43	3.26	0.45	3.37	0.38
50:50	2.17	1.51	2.29	1.74	-	-	2.18	1.63
50:50 (L)	1.76	2.87	1.70	3.09	-	-	1.73	2.18
50:50+Cs	2.36	1.65	2.34	1.65	2.44	1.80	2.17	1.48
50:50+Cs (L)	2.36	2.30	1.96	2.74	1.89	2.94	1.84	1.99
CsFA	2.95	-	2.82	0.17	3.13	0.24	3.10	0.25
CsFA (L)	2.91	-	3.04	0.21	3.01	0.24	3.07	0.24

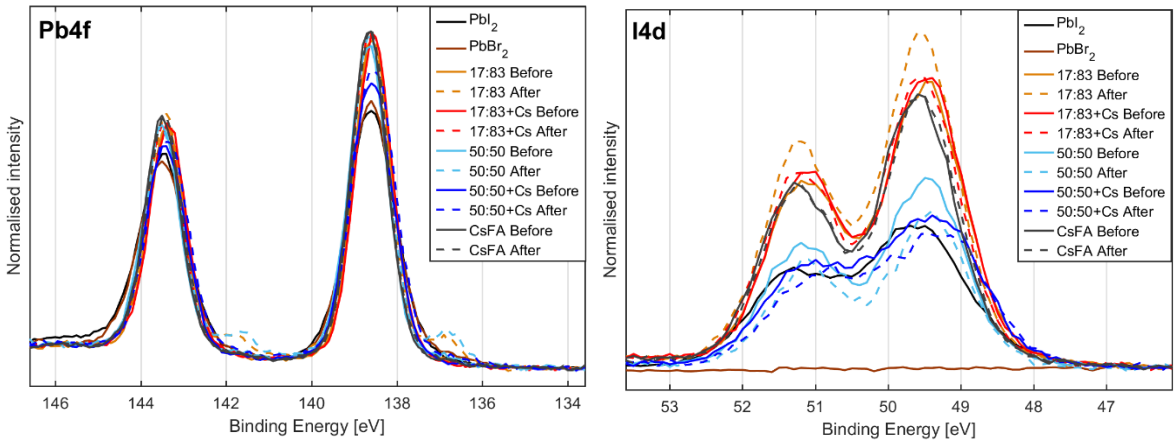

Figure S7: Pb4f and I4d spectra measured at 540 eV normalised to the Pb(II) 4f area and energy calibrated against Pb(II) $4f_{7/2}$ at 138.6 eV. The variation in peak height for Pb4f is due to variations in peak width and background shape.

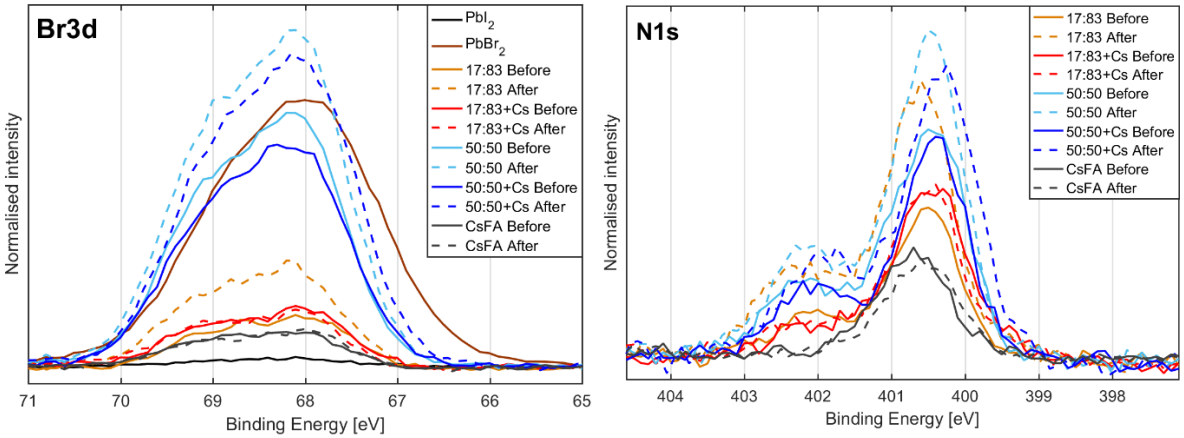

Figure S8: Br3d and N1s spectra measured at 540 eV normalised to the Pb(II) 4f area and energy calibrated against Pb(II) $4f_{7/2}$ at 138.6 eV.

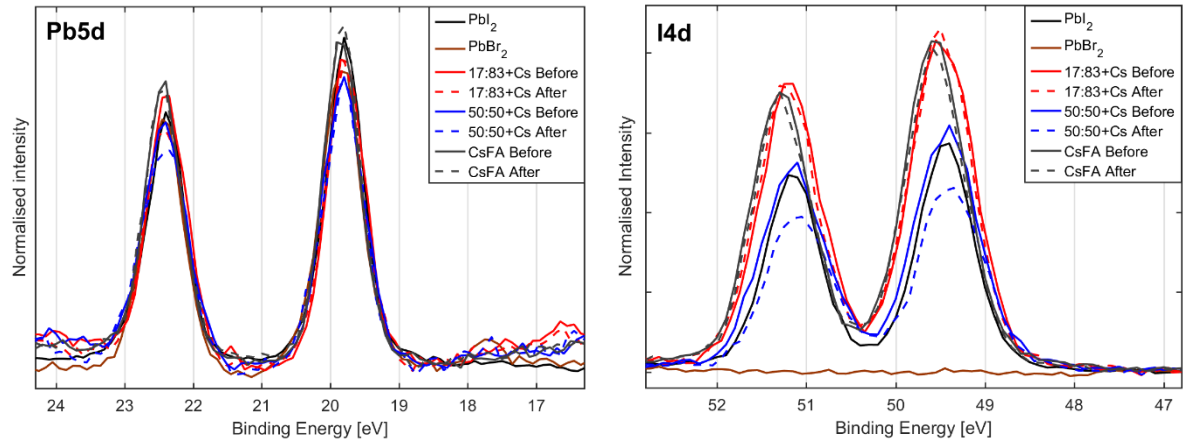

Figure S9: Pb5d and I4d spectra measured at 147 eV normalised to the Pb(II) 5d area and energy calibrated against Pb(II) $5d_{5/2}$ at 19.8 eV. The variation in peak height for Pb5d is due to variations in peak width and background shape.

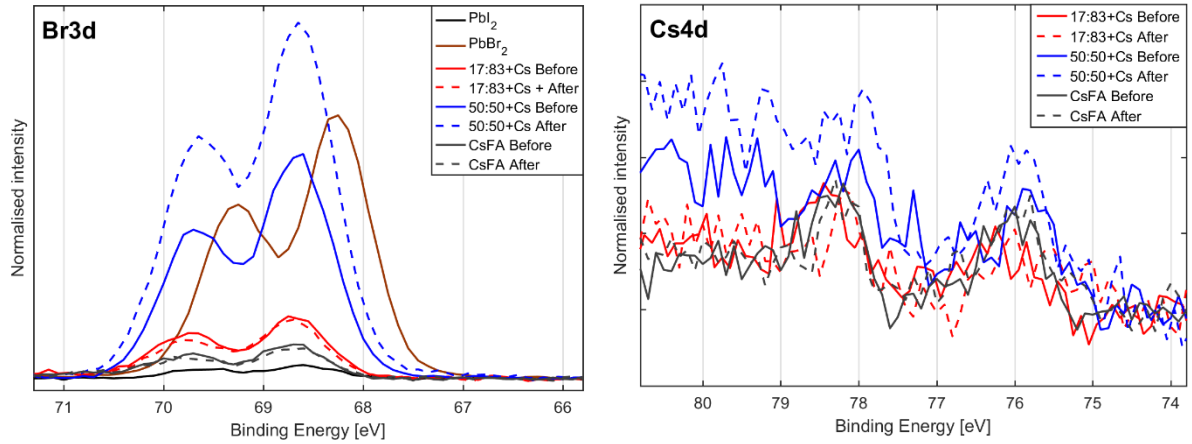

Figure S7: Br3d and Cs4d spectra measured at 147 eV normalised to the Pb(II) 5d area and energy calibrated against Pb(II) $5d_{5/2}$ at 19.8 eV.

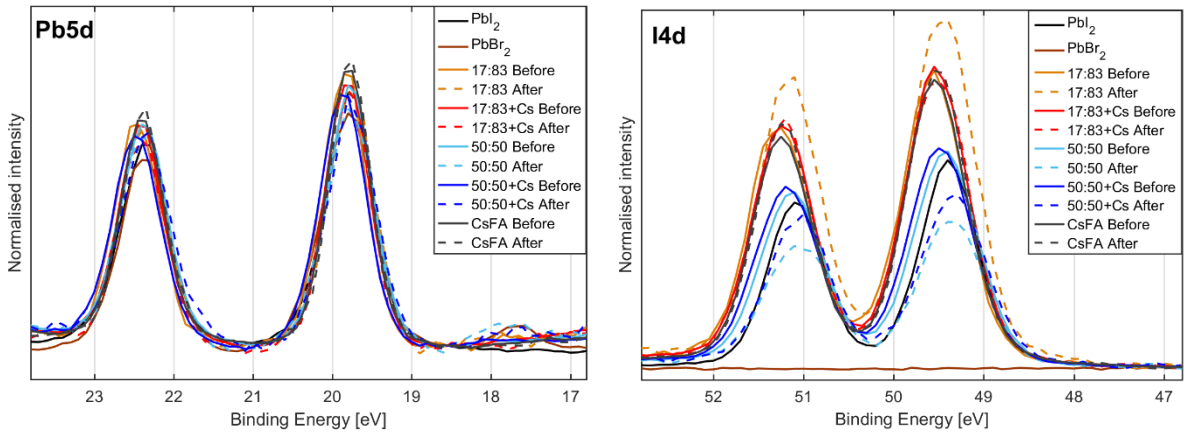

Figure S11: Pb5d and I4d spectra measured at 139 eV normalised to the Pb(II) 5d area and energy calibrated against Pb(II) $5d_{5/2}$ at 19.8 eV. The variation in peak height for Pb5d is due to variations in peak width and background shape.

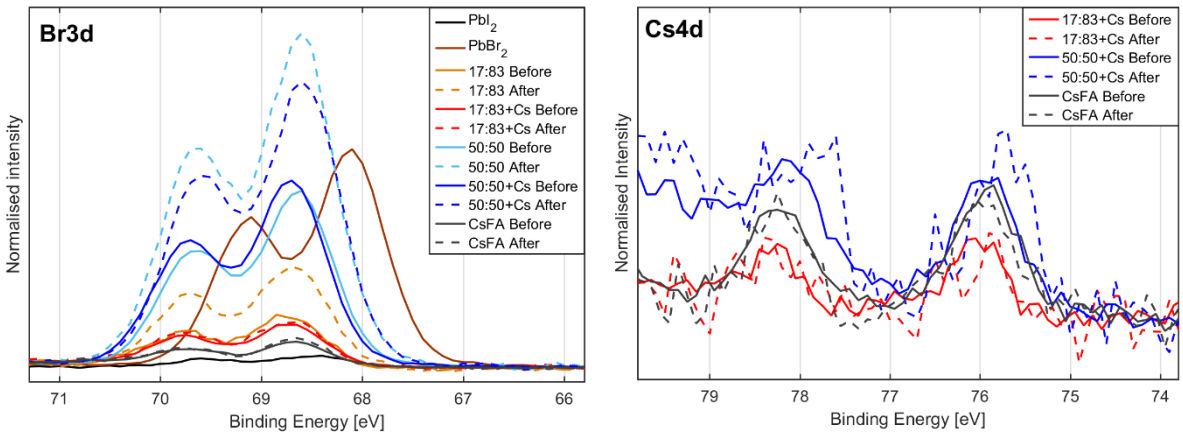

Figure S12: Br3d and Cs4d spectra measured at 139 eV normalised to the Pb(II) 5d area and energy calibrated against Pb(II) $5d_{5/2}$ at 19.8 eV.

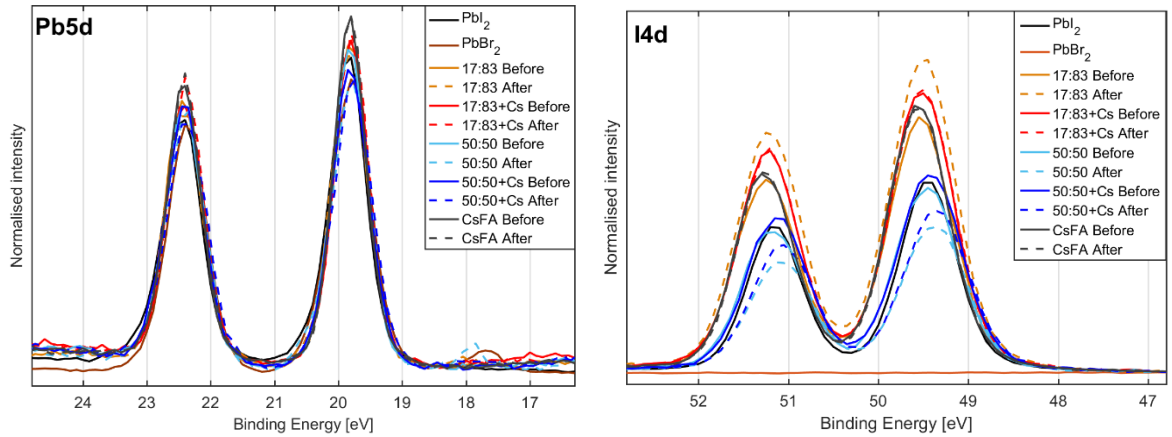

Figure S13: Pb5d and I4d spectra measured at 120 eV normalised to the Pb(II) 5d area and energy calibrated against Pb(II) $5d_{5/2}$ at 19.8 eV. The variation in peak height for Pb5d is due to variations in peak width and background shape.

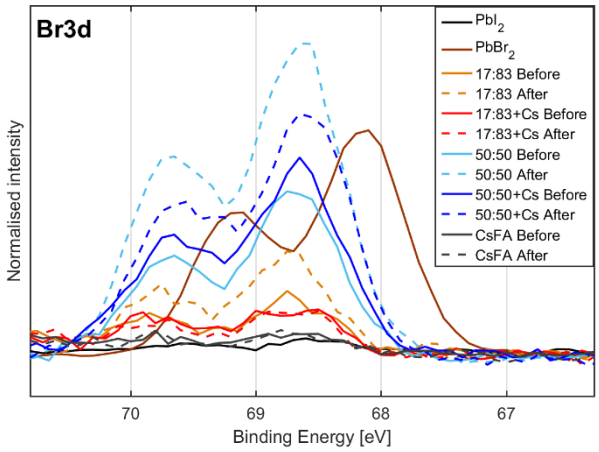

Figure S14: Br3d spectra measured at 120 eV normalised to the Pb(II) 5d area and energy calibrated against Pb(II) $5d_{5/2}$ at 19.8 eV

Spectral evolution before, during and after laser illumination

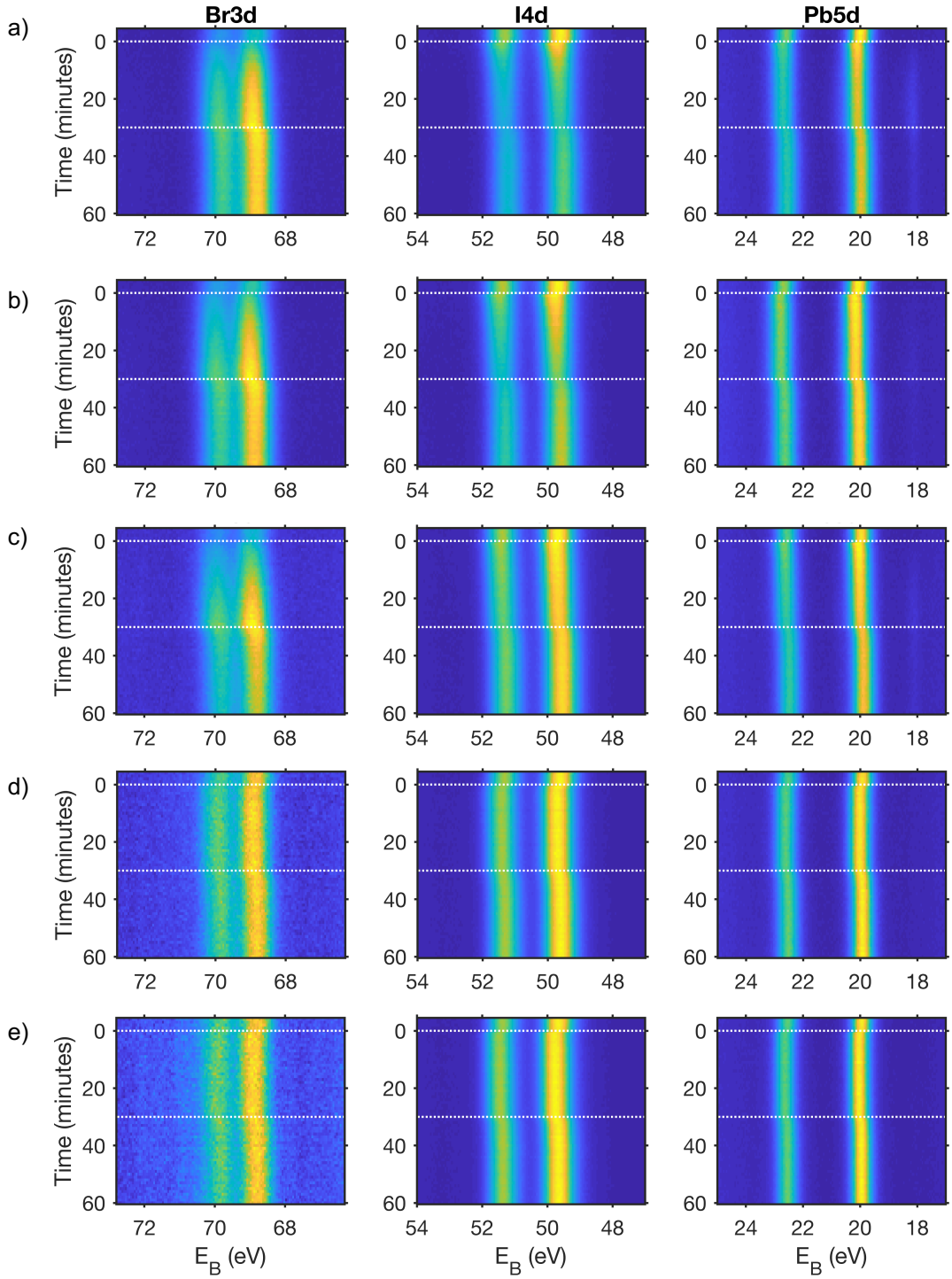

Figure S15: Time evolution of Br3d (left), I4d (middle) and Pb5d (right) spectra measured before, during and after laser illumination with 515 nm and 0.20 mW intensity. White horizontal lines indicate when the laser was switched on and off. The spectra are energy calibrated against the Fermi edge. a) 50:50, b) 50:50+Cs, c) 17:83, d) 17:83+Cs, e) CsFA

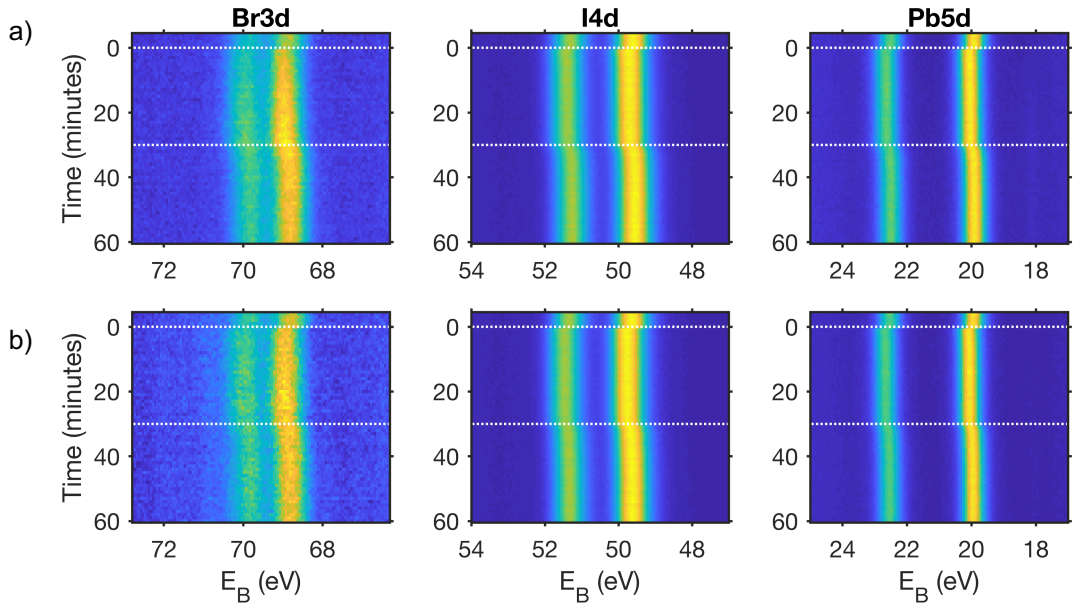

Figure S16: Time evolution of Br3d (left), I4d (middle) and Pb5d (right) spectra measured before, during and after laser illumination with 515 nm and 0.91 mW intensity. White horizontal lines indicate when the laser was switched on and off. The spectra are energy calibrated against the Fermi edge. a) 17:83+Cs, b) CsFA

Peak shifts and sample characterisation

The changes in peak position of the Pb(+II), I(-I) and Br(-I) peaks during 0.91 mW laser illumination are presented in Figure S17. At this higher intensity we observe that the peak shift for CsFA returns to its original position but we do not observe this for 17:83+Cs, indicating that CsFA is more stable than 17:83+Cs.

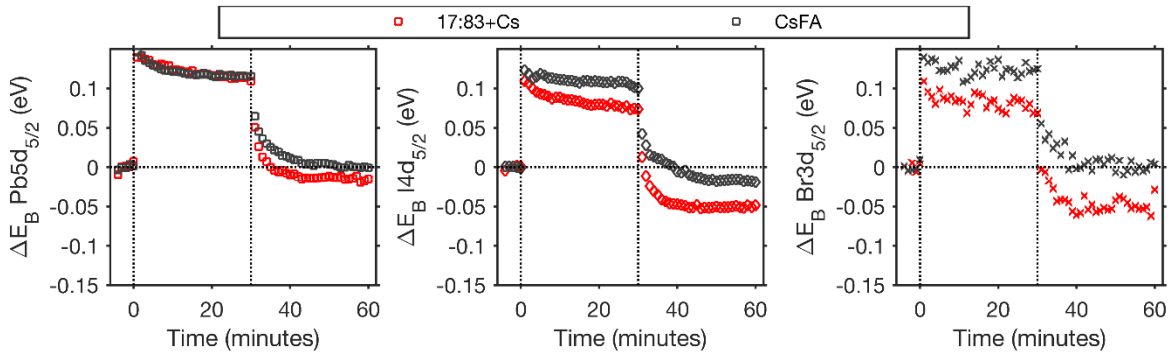

Figure S17: The shift in peak position observed during illumination with 0.91 mW laser illumination relative to the original position. From left to right, Pb5d, I4d and Br3d.

References

[1] F. Giordano *et al.*, "Enhanced electronic properties in mesoporous TiO2 via lithium doping for high-efficiency perovskite solar cells," *Nat. Commun.*, vol. 7, p. 10379, Jan. 2016.

[2] Y. Zhao and K. Zhu, "Solution Chemistry Engineering toward High-Efficiency Perovskite Solar Cells," *J. Phys. Chem. Lett.*, vol. 5, no. 23, pp. 4175–4186, Dec. 2014.

[3] M. Xiao *et al.*, "A Fast Deposition-Crystallization Procedure for Highly Efficient Lead Iodide Perovskite Thin-Film Solar Cells," *Angew. Chem.*, vol. 126, no. 37, pp. 10056–10061, Sep. 2014.

[4] N. J. Jeon, J. H. Noh, Y. C. Kim, W. S. Yang, S. Ryu, and S. I. Seok, "Solvent engineering for high-performance inorganic–organic hybrid perovskite solar cells," *Nat. Mater.*, vol. 13, no. 9, pp. 897–903, Sep. 2014.

[5] A. Abate *et al.*, “Lithium salts as ‘redox active’ p-type dopants for organic semiconductors and their impact in solid-state dye-sensitized solar cells,” *Phys. Chem. Chem. Phys.*, vol. 15, no. 7, p. 2572, 2013.
[6] A. Abate, D. R. Staff, D. J. Hollman, H. J. Snaith, and A. B. Walker, “Influence of ionizing dopants on charge transport in organic semiconductors,” *Phys Chem Chem Phys*, vol. 16, no. 3, pp. 1132–1138, 2014.